Environ. Sci. Technol. **2011,** *45,* 809–814

CO_2 Adsorption on Carbon Models of Organic Constituents of Gas Shale and Coal

YANGYANG LIU AND JENNIFER WILCOX*

Department of Energy Resources Engineering, School of Earth Sciences, Stanford University, Green Earth Sciences 065, 367 Panama Street, Stanford, California 94305, United States

Received August 8, 2010. Revised manuscript received November 22, 2010. Accepted November 23, 2010.

Imperfections of the organic matrix in coal and gas shales are modeled using defective and defect-free graphene surfaces to represent the structural heterogeneity and related chemical nature of these complex systems. Based upon previous experimental investigations that have validated the stability and existence of defect sites in graphene, plane-wave electronic density functional theory (DFT) calculations have been performed to investigate the mechanisms of CO_2 adsorption. The interactions of CO_2 with different surfaces have been compared, and the physisorption energy of CO_2 on the defective graphene adsorption site with one carbon atom missing (monovacancy) is approximately 4 times as strong as that on a perfect defect-free graphene surface, specifically, with a physisorption energy of ~210 meV on the monovacancy site compared to ~50 meV on a perfect graphene surface. The energy associated with the chemisorption of CO_2 on the monovacancy site is substantially stronger at ~1.72 eV. Bader charge, density of states, and vibrational frequency estimations were also carried out and the results indicate that the CO_2 molecule binds to the surface becoming more stable upon physisorption onto the monovacancy site followed by the original C=O bonds weakening upon CO_2 chemisorption onto the vacancy site.

1. Introduction

Annual carbon dioxide (CO_2) emissions from fossil fuel combustion have been increasing exponentially compared to those in the preindustrial era. Globally, approximately 30.4 Gt of CO_2 were added to the atmosphere through the combustion of fossil fuels in 2008, which were almost twice as much as the average emitted throughout the 1970s. Within the U.S., fossil fuel combustion accounted for approximately 94% of CO_2 emissions in 2008 (*1*). Worldwide economic stability and development require energy, which today is largely dominated by the direct combustion of fossil fuels. The total primary energy supply of the world doubled in the last 30 years due to the use of fossil fuels (*2*). With world energy supply (fossil fuels accounting for 81%) expected to rise by 52% between 2004 and 2030, global CO_2 emissions from energy generation is expected to reach 40.4 Gt CO_2/year by 2030 under present policies (*3*). The Intergovernmental Panel on Climate Change (IPCC) indicates the need for an immediate 50−70% reduction in CO_2 emissions to stabilize global CO_2 concentrations at 1990 levels by 2100 (*4*).

Various studies are focused on the potential to capture and store CO_2. After capturing directly from the industrial sources, CO_2 can be transported and injected into geologic formations to minimize global emissions. Different kinds of geologic formations have been proposed and investigated, including unmineable coalbeds, deep saline aquifers, depleted or depleting oil/gas reservoirs, etc., and each have different mechanisms associated with CO_2 storage (*5*). One advantage of storing CO_2 in coalbeds is that they are often close in proximity to electricity generation sources (e.g., CO_2 point sources). Another advantage is that CO_2 injection into coalbeds enhances subsequent methane (CH_4) recovery (*6*). Coalbed methane (CBM) represents more than 10% of technically recoverable natural gas in the U.S. (*7, 8*). The energy byproduct of enhanced coalbed methane production also assists in offsetting the high costs of CO_2 capture and storage (CCS), which could make it an economically viable option.

It is well accepted that coal in addition to the organic components of gas shales are extremely complex matrices comprised of molecular frameworks varying considerably in pore size, shape, and network. Previous studies provide indication that these systems are comprised of aromatic and aliphatic structures and/or other functional groups acting as bridges or comprising the chemical makeup of the pore surfaces (*9, 10*). The presence of volatile components such as water vapor, methane, and nitrogen- and sulfur-containing compounds is also expected. Indeed, these functional groups are expected to play a role in the adsorption mechanisms associated with CO_2 and methane on these systems depending on the local temperature and pressure. For instance, if the temperature and pressure conditions favor surface-bound water or various forms of dissociated water (e.g., hydroxyl or carbonyl groups at the carbon surface) at the surface this may lead to complex CO_2−water−surface interactions. Rather than CO_2 interacting directly with a surface, it may react indirectly via a shared proton. These types of investigations will reveal whether these functional groups will act to passivate or enhance the CO_2-surface adsorption. Future work will involve the investigation of these indirect surface interactions, with the current work focusing specifically on CO_2-surface interactions. Also, it has been reported that at the high pressures associated with sequestration that coal becomes CO_2 wet (*11*), thus providing support to the initial focus on CO_2−surface interactions.

Using electronic structure theory to investigate CO_2 reactivity with defective carbon surfaces may also provide insight into the mechanism associated with the observed plasticization phenomena in ECBM operations. If the coal cleat fractures become restricted because of the coal plasticization, the gas permeability will be changed dramatically (*5, 9*). Electronic structure theory is a molecular-scale analysis, and the understanding of the properties of the adsorbed phase of molecular CO_2 (as opposed to bulk) will assist in setting up models for the initial framework required to carry out statistical modeling such as Monte Carlo (MC). For instance, Grand Canonical MC has been successful at reproducing adsorption phenomena at the bench-scale (*12*). However, the agreement between the MC and experimental adsorption experiments often involve structurally and chemically homogeneous systems such as zeolites and metal−organic frameworks. With the chemistry of the organic matrix unknown in the current systems it is crucial that the initial

* Corresponding author phone: 650 724 9449; fax: 650 725 2099; e-mail: wilcoxj@stanford.edu.

10.1021/es102700c
Published on Web 12/10/2010

models for MC are as representative of the chemistry as possible. For instance, existing models include the slit-pore model with a homogeneous surface of carbon atoms represented by a graphitic structure. Perhaps more realistic models for the complex Earth systems of focus in the current work are defective graphitic surfaces or surfaces with embedded functional groups.

Pore surfaces in coal were modeled previously by various idealized graphitic structures, including single-walled carbon nanotubes (SWNTs) and single graphene layers (*13*−*17*). In addition to CO_2 storage in coalbeds, understanding gas interactions with defective organic surfaces is crucial for the estimation of initial natural gas in-place and production in gas shales. In most gas shales the organic fraction is less than 5%, and typical clay contents range from 30−50%, and the gas is likely to be adsorbed both within the micropores (<2 nm) of the organic fraction, in addition to the interlayer spacing of the clays (*18, 19*).

Within the complex heterogeneous structure of the organic matrices of coal and gas shales there likely exists a combination of defect sites and dangling bonds. Both the pore structure and surface reactivity will influence the mechanism associated with the CO_2-surface interactions and subsequent storage potential. Defect sites are defined in this work as missing-atom sites while dangling bonds are in reference to edge sites. A defect site with a missing carbon atom will leave vacancies in which the carbon atoms at the vacancy are undercoordinated. To a certain extent the charge in this system will redistribute making these carbons slightly negative (possibly balanced by water existing in the local environment), differing from the chemistry and electronic structure of the edge sites, which do not have the influence of localized and symmetric undercoordinated carbon atoms. The focus of the current work will be on defect sites as a first step, whereas future work will investigate the reactivity of edge sites in addition to the influence of functional groups including oxygen, hydrogen, nitrogen, and sulfur atoms.

Although the adsorption of CO_2 on simplified graphitic surfaces has been experimentally and computationally investigated previously over the past several years (*20*−*31*), there are a limited number of theoretical studies that take chemical and structural heterogeneity into account. Xu et al. (*27*) investigated the different dissociative adsorption pathways of CO_2 on a perfect graphite (0001) surface using the first-principles-based B3LYP/6-31+G(d) hybrid density functional method. It was determined in this study that the two oxygen atoms of the CO_2 molecule each react differently with the surface, that is, one oxygen atom was reported to participate in forming an epoxy group, while the other formed either a gas-phase CO molecule (main reaction pathway) or a lactone group. The physisorption energy was reported to be ∼0.7 kcal/mol (∼30 meV), and the chemisorption energy of the main chemical reaction ∼96 kcal/mol (∼416 meV) after CO_2 overcomes a forward barrier of ∼120 kcal/mol (∼520 meV). Density functional theory within the Perdew−Wang 91 (*32*) version of GGA was employed by Cabrera−Sanfelix (*31*) to investigate the adsorption of CO_2 on a defective graphene (0001) sheet with a single vacancy site. The physisorption energy was calculated to be ∼136 meV. Subsequently, chemisorption occurred after overcoming an energy barrier of about 1 eV relative to the gas phase, and a lactone group was formed with an exothermicity of about 1.4 eV. Carbon atoms of the graphene surfaces in this previous work were allowed to relax with the exception of a single carbon atom located at the edge of the small unit cell (4 × 4), which leads to an artificially induced contraction of the lattice during the geometry optimization, and subsequent asymmetric chemisorption of CO_2 onto the monovacancy site.

The objectives of this work were to apply plane-wave electronic density functional theory to gain a more accurate picture of the mechanism of CO_2 adsorption on defective graphene surfaces by investigating the effect of employing different unit-cell sizes with partial or full flexibility of surface carbon atoms, and also to obtain partial charge distribution of defective graphene surfaces to serve as an accurate framework for future work involving adsorption isotherm predictions using statistical-based methods.

2. Computational Methodology

The Vienna *ab initio* simulation package (VASP) (*33, 34*) was used for all calculations and plane-wave electronic density functional theory (DFT) was employed due to its balanced computational efficiency and accuracy. The projector augmented wave (PAW) potential (*35, 36*) was used to describe the core−valence electron interaction of the carbon and oxygen atoms. The Perdew−Wang 1991 (PW91) version of the generalized gradient approximation (GGA) (*32*) was compared to other GGA methods and to the local density approximation (LDA).

An idealized carbon-based pore surface was represented using a graphene slab and a unit cell with periodic boundary conditions along three spatial directions. Previous investigations (*31, 37*) have confirmed that graphene is a sufficient system to model the CO_2-surface interactions within a slit pore of a graphite framework due to the weak influence the neighboring carbon layers have on the adsorption energy. In the current work a vacuum region of 18 Å between periodic basal planes was used, along with 5 × 5 × 1 Monkhorst-Pack (*38*) *k*-point sampling, and a plane-wave cutoff of 400 eV. The perfect graphene basal plane surface and three defective-graphene surfaces each with unique vacancy sites were investigated. Specifically, the following three vacancy sites were studied: the vacancy site with one carbon atom missing (monovacancy or V1) (*39*), the double vacancy (C2), which is comprised of two pentagonal rings and one octagonal ring referred to as the 5−8−5 defect, and the Stone−Wales (SW) defect (5−7−7−5) (*39, 40*) whose importance is often highlighted with respect to its demonstrated mechanical properties in carbon nanotubes and other graphitic materials, which are thought to be responsible for nanoscale plasticity and ductility (*41*). Since the monovacancy site was found to be the most reactive toward CO_2, results associated with this defect site in addition to the defect-free graphene are discussed in detail. A thorough discussion of the adsorption mechanisms associated with CO_2 on the C2 and SW defect sites is available in the Supporting Information (SI). Due to the heterogeneity of the carbon matrix of coal and those comprised of gas shales, it is assumed that defect sites of these types in addition to graphene edge sites could be characteristic of active sites for adsorption on pore surfaces.

The adsorption energies, E_{ads}, can be calculated from eq 1:

$$E_{ads} = E_{surf+CO_2} - E_{surf} - E_{CO_2} \quad (1)$$

where E_{surf} and E_{CO_2} correspond to the total energies of the optimized defective surface and the isolated gas-phase CO_2 molecule, respectively, and $E_{surf+CO_2}$ represents the total energy of the optimized surface-CO_2 system. The CO_2 molecule was initially placed at a certain molecular height with various possible configurations, where it was considered to be noninteracting with the defective surface. The molecular height refers to the distance between the central carbon atom of the CO_2 molecule and a fixed reference carbon atom in the basal plane in the *z*-direction. The physisorption pathway of CO_2 was determined by optimizing the geometry of CO_2 upon a given surface at varying stepwise distances from the

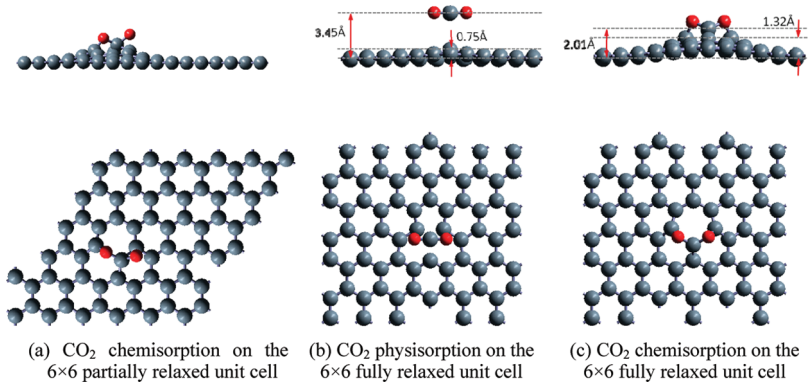

(a) CO_2 chemisorption on the 6×6 partially relaxed unit cell (b) CO_2 physisorption on the 6×6 fully relaxed unit cell (c) CO_2 chemisorption on the 6×6 fully relaxed unit cell

FIGURE 1. Structures of CO_2 physisorption and chemisorption on the monovacancy site using a 6 × 6 unit cell with partial to full flexibility: gray, carbon atoms; red, oxygen atom.

surface. After examining a number of possible pathways with different CO_2 orientations, the CO_2 molecule was allowed to fully relax at each CO_2-surface height considered. The potential energy associated with each CO_2-surface distance was plotted, with the minimum energy representing the CO_2 physisorption energy. The chemisorption state was determined by moving the CO_2 molecule further along the minimum energy path toward the vacancy site to a second potential well (deeper than the first). The potential energy surface plots are presented in the SI.

Vibrational frequencies for gas-phase CO_2, physisorbed and chemisorbed states have been calculated. Density of states, Bader charge, and charge difference analyses were also carried out to further understand the electronic structure of both the defective surface and CO_2−surface complex throughout the adsorption process.

3. Results and Discussion

3.1. Inclusion of All-Atom System Flexibility. Within the current investigation, to determine the characteristics of an isolated vacancy site, a 6 × 6 unit cell was employed to avoid interaction between periodic unit cells that may be encountered using the 4 × 4 unit cell, which was employed by Cabrera−Sanfelix (*31*). Two sets of 6 × 6 unit cells were investigated within the defective graphene surface calculations. Within the first type of the 6 × 6 unit cell, the surface carbon atoms that were nearest and next-nearest neighbors of the vacancy site were allowed full flexibility. The third and fourth nearest-neighbors were fixed in order to minimize elastic interactions between periodic vacancy defects. A second set of 6 × 6 unit-cell calculations were carried out, in which all the surface carbon atoms were allowed full flexibility, providing a more realistic representation. Calculations were also carried out using the small unit cell (4 × 4) and are available in the SI.

The physisorption energies were calculated to be ∼50 meV for CO_2 onto the perfect graphene and ∼210 meV for CO_2 onto the monovacancy site with the 6 × 6 unit cell with full flexibility, which are consistent with the results of ∼51 meV for the perfect graphene and ∼225 meV for the monovacancy site calculated by the 4 × 4 unit cell. However, the chemisorption predictions are different depending on the size of the unit cell used and extent of system flexibility, as shown in Figure 1 (a) and (c). In the current work the CO_2 adsorbs to the defect site in a symmetric fashion, which is expected since CO_2 and the surface are both symmetric systems. All previous studies have concerning CO_2−graphitic surface interactions have postulated asymmetric adsorption behavior of CO_2 on surface defect sites (*27, 31*), which is counterintuitive to what is expected due to the symmetry of the CO_2−surface system. The current work is the first to reveal a symmetric mechanism of adsorption. Therefore, the adsorption mechanisms discussed in the remainder of the manuscript are concerning the 6 × 6 unit cell with all of the surface carbon atoms flexible.

3.2. Adsorption Energy and Structure. The physisorption energy of CO_2 on the monovacancy site is ∼210 meV, and the chemisorption energy is ∼1.72 eV. The details of the CO_2 physisorption calculations for the defect and defect-free graphene surfaces are available in the SI and only the physisorption and chemisorption mechanism of CO_2 on the monovacancy site will be presented in detail. As shown in Figure 1 (b), when CO_2 is physisorbed on the monovacancy site, the molecular height of the CO_2 molecule is 3.45 Å, which is comparable to the DFT results of 3.47 Å predicted by Cabrera−Sanfelix (*31*). Due to the interactions between the adsorbent and adsorbate, the graphene surface carbon atoms move toward the CO_2 molecule, with the height of the highest carbon atom being 0.75 Å. Similarly, as shown in Figure 1 (c), when CO_2 is chemisorbed on the monovacancy site, the height of the previous central carbon atom decreases to 2.01 Å, and the two oxygen atoms of the CO_2 molecule attract the surface carbon atoms allowing them to move upward, resulting in a height of 1.32 Å.

The interaction with defective graphene (monovacancy) surfaces yields stronger CO_2-surface interactions compared to perfect graphene or the other two vacancy sites, that is, 5−7−7−5 and 5−5−8. More specifically, the physisorption energy of CO_2 on the defective graphene site with one carbon atom missing (monovacancy) is approximately 4 times as strong as that on a perfect graphene surface or the other two vacancy sites, 5−7−7−5 and 5−8−5.

3.3. Geometric Structure and Vibrational Frequency Predictions. As shown in Table 2, the bond lengths and bond angle of physisorbed CO_2 changed compared to the gas-phase CO_2 molecule. CO_2 is a linear molecule in the gas phase (*42*); however, when CO_2 is physisorbed, the bond angle becomes ∼178°. The vibrational frequencies of gas-phase CO_2 and physisorbed CO_2 on the monovacancy site were also calculated. The vibrational frequencies of the asymmetric ($\nu 3$) and symmetric stretching ($\nu 1$) modes for gas-phase CO_2 were calculated to be 2360 cm^{-1} and 1321 cm^{-1}, which are comparable to the experimental value of 2349 cm^{-1} and 1333 cm^{-1}, respectively (*42, 43*). The doubly degenerate CO_2 bending frequency ($\nu 2$) for gas-phase CO_2 is calculated to be 638 cm^{-1}, which is comparable to the experimental value of 667 cm^{-1} (*42, 43*). There are slight discrepancies between the DFT-calculated vibrational frequencies and the experimental values, which is fairly typical in quantum chemistry calculations (*44*). The discrepancy between the DFT result and the true vibrational frequency arises in part because of the harmonic treatment of the vibrations, but is also due to the inexact nature of DFT in solving the Schrödinger equation. To correct for this discrepancy, an empirical scaling factor can be applied, with the scaling factors for GGA typically ranging between 0.95 and 0.99 (*44*), which is inline with the

TABLE 1. Perfect and Defective Graphene Surfaces Investigated

Perfect Graphene Surface	Defective Graphene Surfaces		
	Monovacancy	Vacancy 5-7-7-5	Vacancy 5-8-5
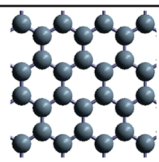	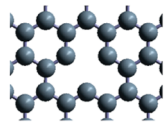	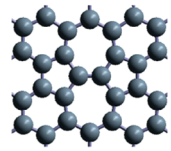	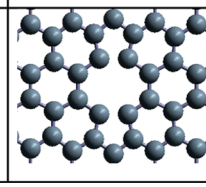

TABLE 2. Geometry and Vibrational Frequency Comparison

		gas-phase			physisorption			chemisorption
		experimental	theoretical	current work	theoretical	experimental	current work	current work
C=O bond length (Å)		1.16 (*42*)		1.176			1.175	1.35 (C−O)
bond angle (degree)		180 (*42*)		180			178	111 (O−C−O)
C=O stretching (cm^{-1})	asymmetric $\nu 3$	2349 (*42, 43*)	2352 (*31*)	2360	2356 (*31*)	2335−2332 (various coals) (*45*) 2326 (C_{60}) (*46*) 2341 (graphite) (*46*)	2353	1319
	symmetric $\nu 1$	1333 (*42, 43*)	1285 (*31*)	1321	1322 (*31*)		1314	1256
C=O bending (cm^{-1})	$\nu 2$	667 (*42, 43*)		638		654/652 (C_{60}) (*46*) 662/657 (graphite) (*47*)	631/588	

scaling required for our predictions to agree with experimental measurements. The calculated C=O asymmetric stretching mode ($\nu 3$) for physisorbed CO_2 of 2353 cm^{-1} is comparable to the value reported in the literature of 2356 cm^{-1} (*31*). This calculated C=O asymmetric stretching mode for physisorbed CO_2 downshifts by 7 cm^{-1} to a slightly lower value compared to the calculated gas-phase CO_2 of 2360 cm^{-1}. In terms of experimental comparison, there are no direct results of CO_2 physisorbed on the graphene monovacancy site, but it is reasonable to compare with CO_2 physisorbed on different coal and other carbon materials since the monovacancy site in addition to other defects are likely to exist in the undercoordinated and heterogeneous carbon frameworks of these systems. The experimental asymmetric stretching frequencies ($\nu 3$) of physisorbed pure CO_2 downshifts to the range of 2335−2332 cm^{-1} for CO_2 adsorbed in various dried coals (*45*) measured using attenuated total reflectance-Fourier transform infrared (ATR-FTIR) spectroscopy as a function of time at constant CO_2 pressure (~0.62 MPa) and temperature (~328.15 K). Downshifts to the value of 2326 cm^{-1} for CO_2 adsorbed on a C_{60} film (crystal sizes in the range of 0.025−0.2 μm), and downshifts to the value of 2341 cm^{-1} for CO_2 on a graphite film (with cavity of 10−30 μm in diameter, and assume CO_2 adsorbs on the basal plane) recorded using Perkin-Elmer 580B Infrared and Nicolet 520 FTIR spectrophotometers at equilibrium pressures less than 100 mTorr (~13.3 Pa) and temperatures in the range of 120−150 K (*46*). To a reasonable approximation, each of the vibrations within the CO_2 molecule can be regarded as a harmonic oscillator, with the vibrational frequency proportional to the square root of the bond's force constant, reflecting the strength of the bond through its magnitude (*47*). The fact that the vibrational frequencies are higher indicate that the C=O bond is stronger when the CO_2 molecule is physisorbed onto the monovacancy site than that physisorbed on the perfect carbon materials like C_{60} and graphite. Upon interaction with the monovacancy site, the doubly degenerate CO_2 bending mode ($\nu 2$) of CO_2 is separated into two different vibrations attributed to the change of symmetry of the molecule, that is, an in-plane bending mode and an out-of-plane bending mode. The bending modes ($\nu 2$) were calculated to be 631/588 cm^{-1} for CO_2 on the monovacancy site. These decoupling bending modes ($\nu 2$) were reported to be 654/652 cm^{-1} for CO_2 on C_{60}, and 662/657 cm^{-1} for CO_2 on graphite (*46*), both showed a downshift compared to the $\nu 2$ mode in the gas phase. The asymmetric ($\nu 3$) and symmetric ($\nu 1$) modes of the C—O bond were calculated to be 1319 cm^{-1} and 1256 cm^{-1}, respectively. These values are much lower than those of the carbon−oxygen double bonds in the CO_2 molecule. Together with the fact that the carbon−oxygen bond length increases, it can be concluded that the C=O bonds are broken when the CO_2 molecule is chemisorbed on monovacancy site. In terms of CO_2 chemisorption on the defective carbon surfaces, high temperature and/or pressure is required to overcome the energy barrier of the chemisorbed state. To the authors' knowledge there exist no experimental vibrational frequency data at the high temperature (may be up to ~330 K) and pressure conditions (may be more than ~5 MPa) (*48*) representative of coal and gas shale at sequestration depths for comparison with the theoretical predictions of the current work.

3.4. Electronic Structure. The change in charge density was plotted for the CO_2 physisorption and chemisorption complexes on the surface with the monovacancy site. Positive values in the change of charge density indicate a gain of electrons, with negative values representing a loss. As shown in Table 3 (a), when CO_2 is physisorbed onto the surface, the reactive surface carbon atom donates electrons to the region between the CO_2 central carbon atom and itself to strengthen the attraction between CO_2 and the surface. In addition, two small regions of electron accumulation appear near both

TABLE 3. Change in Charge Density (Contour) and Bader Charge Analysis for CO_2 Physisorbed on the Monovacancy Site. Black Dots in Contour: Surface Carbon Atoms; Grey Dot in Contour: CO_2 Central Carbon Atom; White Dots in Contour: CO_2 Oxygen Atoms

(a) CO_2 physisorbed on the monovacancy site

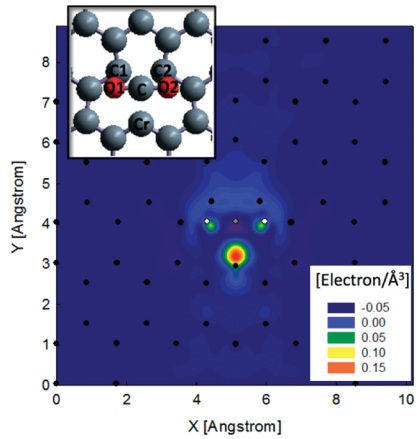

Atom Name	Charge Difference [e]
C1	-0.055
C2	-0.1381
Cr	-0.0506
C	-0.0001
O1	0.0127
O2	0.0162

(b) CO_2 chemisorption on the monovacancy site

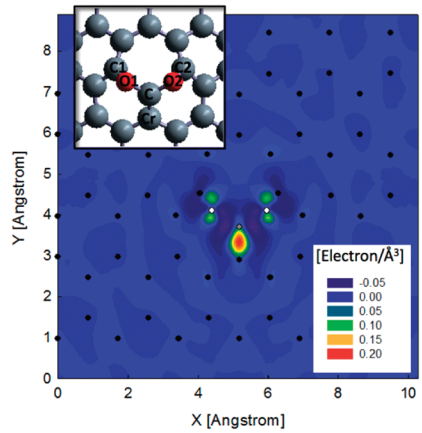

Atom Name	Charge Difference [e]
C1	-0.7614
C2	-0.7298
Cr	-1.5277
C	3.2055
O1	-0.1753
O2	-0.0509

oxygen atoms; therefore, there is higher electron density surrounding CO_2 compared to that of CO_2 in the gas phase, which once again indicates that the CO_2 molecule binds to the surface becoming more stable upon physisorption onto the defect site.

This conclusion generated by the charge difference analysis can also be determined by a Bader charge analysis (*49*). Positive values of a Bader charge analysis represent the gain of electrons compared to that of the original structure, while negative values represent a loss. As shown in Table 3 (a), the reactive surface carbon atom loses 0.05 electrons, and each of the two oxygen atoms gain 0.0178 and 0.006 electrons, respectively, consistent with the results of the change in charge density calculations.

A similar analysis was carried out for CO_2 chemisorption on the monovacancy site. As shown in Table 3 (b), the electron density moves toward the region between the reactive surface carbon atom and the CO_2 central carbon atom, as well as the region between each vacancy carbon atom and oxygen atom. The accumulation of electrons in these regions indicates a new C—C bond and the formation of two C—O bonds. It can also be seen from the profile that electron densities move away from the region between each oxygen atom and the CO_2 central carbon atom, and thus the original C=O bonds are weakened upon CO_2 chemisorption onto the vacancy site. Within both scenarios, the defect site seems to allow for enhanced electron transport and versatility depending on the acid—base nature of the adsorbate, with one defect carbon atom acting as a Lewis base donating its electron density to the carbon atom of CO_2 and the other two defect carbon atoms acting as Lewis acids withdrawing electron density from the two oxygen atoms of CO_2.

Again, using the Bader charge analysis, as shown in Table 3 (b), the CO_2 central carbon atom gains electrons while the reactive surface carbon atom lose electrons, which is consistent with the fact that a new C—C bond forms. In addition, each vacancy carbon atom donates electrons to form a new C—O bond. In its final chemisorbed state, the CO_2 molecule is chemisorbed on the defective graphene surface.

Our current work suggests that CO_2 bonds stronger to the defective graphene surface than perfect graphene. Understanding the mechanism by which CO_2 adsorbs on defective graphene surfaces will ultimately provide insight into not only the mechanism associated with potential long-term storage of CO_2 in coalbeds and gas shales and the feasibility of these strategies as carbon abatement options, but also an idea for screening and designing of organic porous materials for CO_2 capture. Additionally, these focused CO_2-surface investigations may provide insight into the mechanism by

which coal may plasticize upon CO_2 interaction. For the application of CO_2 storage, the existence of H_2O may affect the partial charge distribution of the vacancy sites, and this effect will be investigated in the future work.

Acknowledgments

This research is funded by the Stanford University Graduate Fellowship Program in the School of Earth Sciences. We thank Dr. Anthony Kovseck and Dr. Mark Zoback for their helpful discussions and insight on this work. The computations were carried out on the Center for Computational Earth & Environmental Science (CEES) cluster at Stanford University.

Supporting Information Available

Additional information including Figures S1−S7 and Tables S1−S4. This material is available free of charge via the Internet at http://pubs.acs.org.

Literature Cited

(1) *Inventory of U.S. Greenhouse Gas Emissions and Sinks: 1990−2008*; U.S. Environmental Protection Agency: Washington, DC, 2010.

(2) Quadrelli, R.; Peterson, S. The energy-climate challenge: Recent trends in CO_2 emissions from fuel combustion. *Energy Policy* **2007**, *35*, 5938–5952.

(3) Wang, F. Y.; Zhu, Z. H.; Massarotto, P.; Rudolph, V. Mass transfer in coal seams for CO_2 sequestration. *AIChE J.* **2007**, *53*, 1028–1049.

(4) Intergovernmental Panel on Climate Change: Second Assessment Report: Climate Change 1995. Available at http://www.ipcc.ch/publications_and_data/publications_and_data_reports.htm.

(5) Benson, S.; Cook, P. *Intergovernmental Panel on Climate Change, Special Report on Carbon dioxide Capture and Storage: Underground Geological Storage*, Chapter 5; Cambridge University Press: Cambridge, UK, 2005; pp 196−276.

(6) Khoo, H. H.; Tan, R. B. H. Life cycle investigation of CO_2 recovery and sequestration. *Environ. Sci. Technol.* **2006**, *40*, 4016–4024.

(7) *Annual Energy Outlook, 2009*; U.S. Department of Energy: Washington, DC, 2009.

(8) Orr, F. M., Jr. CO_2 capture and storage: Are we ready. *Energy Environ. Sci.* **2009**, *2*, 449–458.

(9) White, C. M.; Smith, D. H.; Jones, K. L.; Goodman, A. L.; Jikich, S. A.; LaCount, R. B.; et al. Sequestration of carbon dioxide in coal with enhanced coalbed methane recovery—A review. *Energy Fuels* **2005**, *19*, 659–724.

(10) Haenel, M. W. Recent progress in coal structure research. *FUEL* **1992**, *71*, 1211–1223.

(11) Mazumder, S.; Plug, W.-J. Capillary pressure and wettability behavior of coal-water-carbon dioxide system; *SPE Annual Technical Conference and Exhibition*, Denver, CO, 5−8 October, 2003,

(12) Frenkel, D.; Smit, B. *Understanding Molecular Simulation*, 2nd ed.; Academic Press: New York, November, 2001.

(13) Bhatia, S. K.; Tran, K.; Nguyen, T. X.; Nicholson, D. High-pressure adsorption capacity and structure of CO_2 in carbon slit pores: theory and simulation. *Langmuir* **2004**, *20*, 9612–9620.

(14) Cui, X.; Bustin, R. M.; Dipple, G. Selective transport of CO_2, CH_4, and N_2 in coals: insights from modeling of experimental gas adsorption data. *Fuel* **2004**, *83*, 293–303.

(15) Kurniawan, Y.; Bhatia, S. K.; Rudolph, V. Simulation of binary mixture adsorption of methane and CO_2 at supercritical conditions in carbons. *AIChE J.* **2006**, *52* (3), 957–967.

(16) Tenney, C. M.; Lastoskie, C. M. Molecular simulation of carbon dioxide adsorption in chemically and structurally heterogeneous porous carbons. *Environ. Prog.* **2006**, *25* (4), 343–354.

(17) Kowalczyk, P.; Furmaniak, S.; Gauden, P. A.; Terzyk, A. P. Carbon dioxide adsorption-induced deformation of microporous carbons. *J. Phys. Chem. C* **2010**, *114*, 5126–5133.

(18) Bustin, A. M. M.; Bustin, R. M. Importance of Fabric on the Production of Gas Shales, SPE 114167; *SPE Unconventional Reservoirs Conference*, 10-12 February 2008, Keystone, Colorado, 2008.

(19) Ross, D. J. K.; Bustin, R. M. The importance of shale composition and pore structure upon gas storage potential of shale gas reservoirs. *Mar. Petrol. Geol.* **2008**, *26*, 916.

(20) Zhao, J. J.; Buldum, A.; Han, J.; Lu, J. P. Gas molecule adsorption in carbon nanotubes and nanotube bundles. *Nanotechnology* **2002**, *13* (2), 195–200.

(21) Yim, W. L.; Byl, O.; Yates, J. T.; Johnson, J. K. Vibrational behavior of adsorbed CO_2 on single-walled carbon nanotubes. *J. Chem. Phys.* **2004**, *120* (11), 5377–86.

(22) Matranga, C.; Chen, L.; Smith, M.; Bittner, E.; Johnson, J. K.; Bockrath, B. Trapped CO_2 in Carbon Nanotube Bundles. *J. Phys. Chem. B* **2003**, *107*, 12930–12941.

(23) Matranga, C.; Chen, L.; Bockrath, B.; Johnson, J. K. Displacement of CO_2 by Xe in single-walled carbon nanotube bundles. *Phys. Rev. B* **2004**, *70* (165416), 1–7.

(24) Cinke, M.; Li, J.; Bauschlicher, C. W.; Ricca, A.; Meyyappan, M. CO_2 adsorption in single-walled carbon nanotubes. *Chem. Phys. Lett.* **2003**, *376*, 761–766.

(25) Jiang, J. W.; Sandler, S. I. Separation of CO_2 and N_2 by adsorption in C168 Schwarzite: A combination of quantum mechanics and molecular simulation study. *J. Am. Chem. Soc.* **2005**, *127*, 11989–11997.

(26) Chen, L.; Johnson, J. K. Formation of odd-numbered clusters of CO_2 adsorbed on nanotube bundles. *Phys. Rev. Lett.* **2005**, *94* (12), 125701.

(27) Xu, S. C.; Irle, S.; Musaev, D. G.; Lin, M. C. Quantum chemical prediction of reaction pathways and rate constants for dissociative adsorption of CO_x and NO_x on the graphite (0001) surface. *J. Phys. Chem. B* **2006**, *110* (42), 21135–21144.

(28) Rivera, J. L.; McCabe, C.; Cummings, P. T. Layering behavior and axial phase equilibria of pure water and water + carbon dioxide inside single carbon nanotubes. *Nano Lett.* **2002**, *2*, 1427–1431.

(29) Allouche, A.; Ferro, Y. Dissociative adsorption of small molecules at vacancies on the graphite (0001) surface. *Carbon* **2006**, *44*, 3320–3327.

(30) Montoya, A.; Mondragon, F.; Truong, T. N. CO_2 adsorption on carbonaceous surface: A combined experimental and theoretical study. *Carbon* **2003**, *41*, 29–39.

(31) Cabrera-Sanfelix, P. Adsorption and reactivity of CO_2 on defective graphene sheets. *J. Phys. Chem. A* **2009**, *113* (2), 493–498.

(32) Perdew, J. P.; Wang, Y. Accurate and simple analytic representation of the electron-gas correlation energy. *Phys. Rev. B* **1992**, *45*, 13244–13249.

(33) Kresse, G.; Furthmüller, J. Efficiency of ab initio total energy calculations for metals and semiconductors using a plane-wave basis set. *Comput. Mater. Sci.* **1996**, *6*, 15–50.

(34) Kresse, G.; Hafner, J. Ab initio molecular dynamics for open-shell transition metals. *Phys. Rev. B* **1993**, *48*, 13115–13118.

(35) Blöchl, P. E. Projector augmented-wave method. *Phys. Rev. B* **1994**, *50*, 17953–17979.

(36) Kresse, G.; Joubert, D. From ultrasoft pseudopotentials to the projector augmented-wave method. *Phys. Rev. B* **1999**, *59*, 1758–1775.

(37) Sanfelix, P. C.; Holloway, S.; Kolasinski, K. W.; Darling, G. R. The structure of water on the (0 0 0 1) surface of graphite. *Surf. Sci.* **2003**, *532−535*, 166–172.

(38) Monkhorst, H. J.; Pack, J. D. Special points for Brillouin-zone integrations. *Phys. Rev. B* **1976**, *13*, 5188–5192.

(39) Hashimoto, A.; Suenaga, K.; Gloter, A.; Urita, K. Direct evidence for atomic defects in graphene layers. *Nature* **2004**, *430* (19), 870–873.

(40) Kudin, K. N.; Ozbas, B.; Schniepp, H. C.; Prud'homme, R. K.; Aksay, I. A.; Car, R. Raman spectra of graphite oxide and functionalized graphene sheets. *Nano Lett.* **2008**, *8* (1), 36–41.

(41) Ertekin, E.; Chrzan, D. C. Topological description of the Stone-Wales defect formation energy in carbon nanotubes and graphene. *Phys. Rev. B* **2009**, *79*, 155421.

(42) *CRC Handbook of Chemistry and Physics*, 90th ed.; CRC Press: Boca Raton, FL, 2009−2010; 9−33.

(43) Person, W. B.; Zerbi, G. *Vibrational Intensities in Infrared and Raman Spectroscopy*; Elsevier: Amsterdam, 1982.

(44) Sholl, D. S.; Steckel, J. A. *Density Functional theory*; John Wiley & Sons, Inc.: Hoboken, NJ, 2009; 209−233.

(45) Goodman, A. L.; Favors, R. N.; Larsen, J. W. Argonne coal structure rearrangement caused by sorption of CO_2. *Energy Fuels* **2006**, *20* (6), 2537–2543.

(46) Fastowa, M.; Kozirovskia, Y.; Folman, M. IR spectra of CO_2 and N_2O adsorbed on C_{60} and other carbon allotropes - a comparative study. *J. Electron Spectrosc. Relat. Phenom.* **1993**, *64−65*, 843–848.

(47) Hollas, J. M. *Modern spectroscop*, 4th ed.; John Wiley & Sons Ltd.: UK, 2004; 137−197.

(48) Pashin, J. C.; McIntyre, M. R. Temperature-pressure conditions in coalbed methane reservoirs of the Black Warrior basin: implications for carbon sequestration and enhanced coalbed methane recovery. *Int. J. Coal. Geol.* **2003**, *54*, 167–183.

(49) Bader, R. F. W. *Atoms in Molecules: A Quantum Theory*; Oxford University Press: New York, 1990.

ES102700C